ENVIRONMENTAL CHEMISTRY

Microbial synthesis of highly dispersed PdAu alloy for enhanced electrocatalysis

10.1126/sciadv.1600858

Jiawei Liu,[1]* Yue Zheng,[2]* Zilan Hong,[1] Kai Cai,[1] Feng Zhao,[2]† Heyou Han[1]†

Biosynthesis based on the reducing capacity of electrochemically active bacteria is frequently used in the reduction of metal ions into nanoparticles as an eco-friendly way to recycle metal resources. However, those bionanoparticles cannot be used directly as electrocatalysts because of the poor conductivity of cell substrates. This problem was solved by a hydrothermal reaction, which also contributes to the heteroatom doping and alloying between Pd and Au. With the protection of graphene, the aggregation of nanoparticles was successfully avoided, and the porous structure was maintained, resulting in better electrocatalytic activity and durability than commercial Pd/C under both alkaline (CH_3CH_2OH, 6.15-fold of mass activity) and acidic (HCOOH, 6.58-fold of mass activity) conditions. The strategy developed in this work opens up a horizon into designing electrocatalysts through fully utilizing the abundant resources in nature.

INTRODUCTION

Direct liquid fuel cell is considered a promising green energy device for the conversion of chemical energy into electricity because of its high overall electric power efficiency, excellent fuel flexibility, and environmental friendliness (*1*–*3*). Despite its renewable and convenient features, the further development of direct liquid fuel cell is hindered by the low energy conversion efficiency of commercial Pt/C catalysts with relatively low catalytic activity, poor durability, and high cost. Therefore, enormous efforts have been made to seek alternatives to current commercial catalysts in the past few decades (*4*–*10*).

Several strategies have been proposed to enhance the performance of electrocatalysts. First, binary alloy nanocatalysts are fabricated by alloying Pd or Pt with other transition metals, such as PtAu, PdCu, PdNi, PdAu, and PdPtAg (*11*–*15*). Moreover, several nonmetals have also been used as dopants into noble metals, including Pd-P, Pd-Ni-P, and Pt-Ni-P (*16*–*18*). Multialloys are proven to enhance the catalytic activity through the regulation of the surface electronic structure of the catalytic metal by alloying other elements. Another effective strategy to enhance the catalytic activity per unit is seeking and exploiting novel catalyst substrates (such as carbon substrates) with chemical doping (*19*–*24*). Among various element dopings, nitrogen doping is frequently used to enhance the electric conductivity of carbon materials and induce n-type semiconductor property (*25*–*27*). In addition, numerous efforts have also been made to find an efficient way to anchor nanoparticles on those supports (*21*). Traditional methods of chemical synthesis can successfully fabricate alloy catalysts, but the addition of toxic surfactant, stabilizer, and reducing agents makes the synthesis process complicated and environmentally unfriendly, which violates the concept of "green energy." Those capping agents around the nanoparticles may severely limit the activity of catalysts (*28*).

How to fabricate advanced electrocatalysts by a more facile and green method encourages us to develop an alternative protocol from a microbial perspective. It has been reported that metal nanoparticles can be green-synthesized by the metal-respiring bacterium for dechlorination of environmental contaminants and Heck coupling reaction (*29*–*32*). However, the nanoparticles synthesized by microorganisms have rarely been used as electrocatalysts because of the poor conductive nature of microbial cells (*33*). High-temperature carbonization reaction is a common way to increase the conductivity of microbial cells (*33*–*35*), but it cannot avoid the aggregation of those nanoparticles at a high loading amount, limiting their catalytic performance (*33*). Therefore, maintaining the balance between increasing the conductivity of microbial cells and avoiding the aggregation of nanoparticles still remains a challenge to be solved.

To solve the aforementioned problems and develop an efficient electrocatalyst for small organic molecular electrooxidation through a green protocol, this study in situ–synthesized bio-PdAu nanoparticles on the surface of an electrochemically active bacterium without adding toxic surfactant, stabilizer, chemical reductant, and bonding agent. In this process, electrochemically active bacterium served as (i) a reducing agent, (ii) a supporting material, and (iii) doping heteroatom sources at the same time. The as-prepared core/shell bacteria/PdAu (BPA) was further coated by graphene oxide (GO) to form a three-dimensional (3D) core/shell/shell bacteria/PdAu/GO hybrid biofilm (BPAGB). Finally, the doping process, carbonization of bacteria, and reduction of GO were carried out through a facile hydrothermal reaction, and the as-prepared hybrid biofilm became a 3D porous heteroatom-doped bio-PdAu/reduced GO (rGO) hybrid (DPARH) with clean surface and excellent conduction. With the protection of graphene, the aggregation of nanoparticles was successfully avoided under this synergistic condition. The green-synthesized DPARH shows superior electrocatalytic activity and durability and can markedly accelerate the energy conversion on the anode of a direct liquid fuel cell.

RESULTS AND DISCUSSION

Shewanella oneidensis MR-1, a typical electrochemically active bacterium, was used to reduce the metal ions (Pd and Au) and biosynthesize Pd-Au nanoparticles located on the surface of the bacteria. According to previous works, various kinds of metal nanoparticles can be biosynthesized by microorganisms through extracellular electron transfer (*36*). From the perspective of extracellular electron transfer, previous studies

[1]State Key Laboratory of Agricultural Microbiology, College of Science, College of Food Science and Technology, Huazhong Agricultural University, Wuhan 430070, China. [2]Key Laboratory of Urban Pollutant Conversion, Institute of Urban Environment, Chinese Academy of Sciences, Xiamen 361021, China.
*These authors contributed equally to this work.
†Corresponding author. Email: hyhan@mail.hzau.edu.cn (H.H.); fzhao@iue.ac.cn (F.Z.)

proposed the following two principal mechanisms of metal respiration. First, electrons could be directly delivered from the bacterium to the metal ions via either membrane cytochromes or electrically conductive bionanowires. Second, soluble redox molecules, such as flavin, serve as mediators in an indirect electron transfer from the bacteria to the metal ions (*31*). Here, cells of *S. oneidensis* MR-1 were collected by washing to remove residual extracellular compounds to avoid the occurrence of indirect metal reduction. Considering the enrichment medium (LB) consisting of abundant nutrient elements, *Shewanella* cells are not easily apt to generate bionanowires to achieve electron transfer under nutrient-rich environments (*37*). On the basis of experimental procedures and our results, membrane cytochromes might play a main role in metal reduction for biosynthesis of PdAu nanoparticles. Because the complex with OmcA and MtrC of *S. oneidensis* MR-1 has been proven to be the terminal reductase that is crucial for extracellular reduction (*38*), the cells of the mutant (without OmcA and MtrC) were used as a compared experiment. Compared with the reducing performance of the ΔOmcA/MtrC mutant, the native *S. oneidensis* MR-1 showed a stronger reduction with Pd and Au ions (fig. S1). Therefore, the OmcA/MtrC complex worked as one of the key outer membrane proteins in this process, which means that the direct electron transfer of the membrane cytochrome would be the key to biosynthesis of PdAu nanoparticles.

The target material was fabricated in the following three steps (Scheme 1). First, inspired by the redox capacity of the electrochemically active bacterium, the synthesis process started separately with the in situ bioreduction of Pd and Au nanoparticles on the cytomembrane of *S. oneidensis* MR-1, respectively. Second, the BPA was further coated by GO to form a 3D structure, which largely enhanced the specific surface area, as well as stably anchored the PdAu nanoparticles in the middle layer between the bacteria and GO. Meanwhile, the self-assembled sandwich structure coated by GO was constructed to further maintain the bionanoparticles from aggregation after a hydrothermal reaction. Finally, the as-prepared hybrid biofilm was mildly hydrothermally reacted to improve the conductivity of the cell substrate. On the basis of these steps, DPARH was successfully green-synthesized.

The formation process of DPARH electrocatalyst was observed by scanning electron microscopy (SEM) imaging to demonstrate the growth mechanism. Pd nanoparticles were relatively uniformly distributed on the membrane of *S. oneidensis* MR-1 (Fig. 1A) in the first stages. The nanoparticles were densely distributed after reacting with $AuCl_4^-$ (Fig. 1B). The cells with nanoparticles were connected to form 3D network structures by GO coating (Fig. 1C). After the hydrothermal reaction, the skeleton of the cells was reduced in size because of the release of enchylema under high temperature, but the porous structure was still obviously maintained, and PdAu nanoparticles did not aggregate clearly, which is much better than KOH activation at 420°C (temperature ramp, 3°C/min) for 3 hours under argon flow from the same raw materials (Fig. 1D and fig. S2A) (*33*).

Considering the attractive nanostructure and properties of DPARH, we investigated the electrocatalytic activity of this catalyst toward small organic molecular oxidation, including ethanol and formic acid. The as-prepared catalyst showed a much higher electrocatalytic activity and durability than commercial Pd/C under both alkaline (CH_3CH_2OH, 6.15-fold mass activity and 5.8-fold area activity) and acidic (HCOOH, 6.58-fold mass activity and 6.33-fold area activity) conditions (Fig. 2) and performed much better than many other catalysts reported in recent studies (table S1). What leads to the excellent performance of electrooxidation inspired us to further explore the features of this designed catalyst from space structure and composition to surface electronic structure.

The more detailed structure information of BPAGB and DPARH is presented in the following transmission electrion microsopy (TEM) and high-angle annular dark-field scanning TEM (HAADF-STEM) elemental mapping images. The high-resolution TEM (HRTEM) imaging demonstrated that BPAGB consists of small primary nanoparticles with an average diameter of 4.95 nm (Fig. 3A2), and the diameter of DPARH is slightly increased to 6.61 nm (Fig. 3B2). By comparing this with the TEM images of heteroatom-doped bio-PdAu (DPA) (fig. S2B), it can be seen that PdAu nanoparticles are easy to aggregate with each other to form a much larger structure without the protection of GO. The lattice planes with an interplanar distance of about 2.25 and 2.36 Å, which are considered as the (111) plane of face-centered cubic (fcc) metallic Pd and Au, are distributed in different nanoparticles of BPAGB, indicating that Pd and Au nanoparticles are separated from each other (Fig. 3A3). However, the interplanar distance of 2.30 and 2.01 Å, considered as the (111) and (200) planes of fcc metallic PdAu, are found in DPARH, indicating that PdAu nanoparticles become alloy after hydrothermal reaction. To directly prove this phenomenon, the microview was further illustrated by the HAADF-STEM elemental mapping. Pd and Au

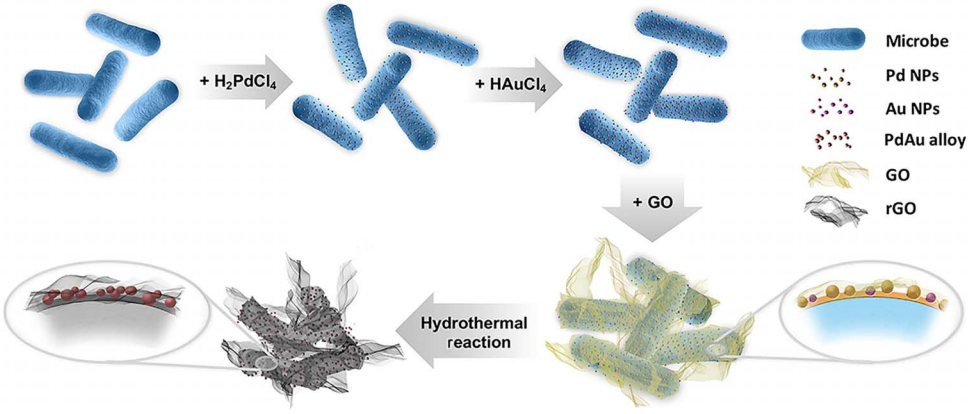

Scheme 1. Formation mechanism for DPARH. NPs, nanoparticles.

nanoparticles were separated on the membrane of cells (Fig. 3, B2 and B3), but they fused together to form an alloy after the hydrothermal reaction (Fig. 3, D2 and D3). When mapping other elements, including P, S, and N, we found that P and S were doped into the metal nanoparticles because heteroatom doping benefits the electrocatalytic performance of catalysts, as reported in previous studies (*16*). On the basis of the location of P and S, the P and S elements may be mainly derived from redox proteins coated on the cells during the metal reduction of biosynthesis. Those membrane proteins participate in the biosynthesis of metal nanoparticles as a reductant and are bound with metal nanoparticles simultaneously. In addition, this phenomenon meant that the membrane protein not only participates in the reducing and supporting process but also plays a crucial role in doping heteroatom into our catalyst, which extends the function of bacteria in three ways: (i) reducing metal ions, (ii) supporting material, and (iii) doping heteroatom. More accurate changes of the structure were further analyzed by powder x-ray diffraction (XRD) pattern.

Figure 4 shows the XRD patterns of *S. oneidensis* MR-1, BPAGB, and DPARH. The Pd and Au reflection peaks are separated in BPAGB, further proving that they are two separated phases in this stage. As to DPARH, there is only a series of peaks corresponding to the cubic phase of PdAu alloy, indicating that the nanoparticles in DPARH are a PdAu alloy rather than Pd or Au nanoparticles, which is in accordance with the result of HAADF-STEM elemental mapping (*39*).

The change in the surface electronic structure of Pd and nitrogen bonding configurations in PBABG and DPARH was investigated by x-ray photoelectron spectroscopy (XPS), as shown in Fig. 5. The binding energies of Pd $3d_{5/2}$ and Pd $3d_{3/2}$ for DPARH are 335.48 and 340.78 eV, respectively, which are evidently higher than those for PBABG (335.18 and 340.58 eV, respectively), and positively shifted to higher binding energy after hydrothermal reaction. The movement of binding energy in Pd indicates the obvious change in the electronic structure of as-prepared materials because of intra- or interatomic charge transfer between Pd and Au when they are alloyed in the DPARH, which might enhance the activity and durability of electrocatalytic ethanol and formic acid oxidation reaction (*40*). Moreover, the high-resolution peak of N1s in BPABG and DPARH could be divided into two characteristic peaks corresponding to pyridinic N and pyrrolic N. It is well known that pyridinic N, pyrrolic N, and graphitic (or quaternary) N are the three main types of nitrogen moiety, and the former two are the two common types that can be found in most of the N-doped graphene treated by hydrothermal reaction (*41*–*46*). With the addition of urea in the reaction, the quaternary N is more likely to be observed in the products (*45*, *46*). Because there is no urea in our hydrothermal reaction, there are therefore only two common types of nitrogen moiety (pyridinic N and pyrrolic N) in our as-prepared catalyst. As previously reported, the pyridinic N (399.14 and 398.35 eV) resulted in a p-electron in the graphene layers to form a p-conjugated system. Because of the contribution of pyridine and pyrrol functionalities, the pyrrolic N (399.89 and 399.6 eV) contributed two p-electrons to the p system (*47*). The pyridinic N content was higher in DPARH, indicating that the nitrogen bonding configurations changed during the hydrothermal reaction, which benefits the electrocatalytic activity of the catalyst (*48*). In addition, the XPS test of DPARH from 0 to 600 eV was also carried out to obtain the semiquantitative atomic ratio of Pd, Au, P, N, and S elements, which can be calculated by the following equation: $n_i/n_j = (I_i/S_i)/(I_j/S_j)$, where n denotes the concentration of atom, I denotes the intensity of photoelectrical peak area, and S denotes the relative atomic

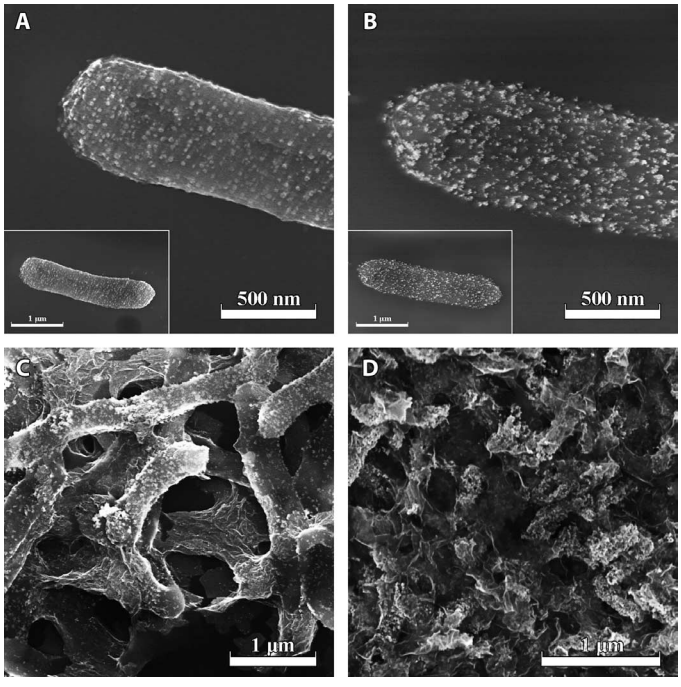

Fig. 1. Morphological features of as-prepared materials in biosynthesis process. SEM images of (**A**) core/shell bacteria/Pd (BP), (**B**) BPA, (**C**) BPABG, and (**D**) DPARH.

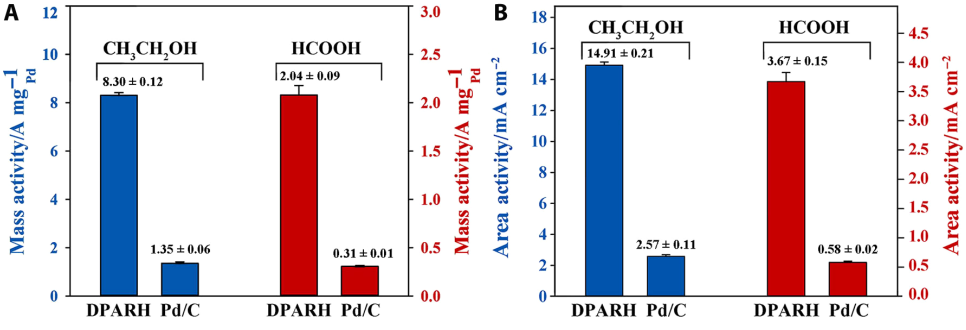

Fig. 2. General electrocatalytic activities of optimized catalyst. Mass activities of DPARH and commercial Pd/C catalysts in CH_3CH_2OH and HCOOH electrooxidation.

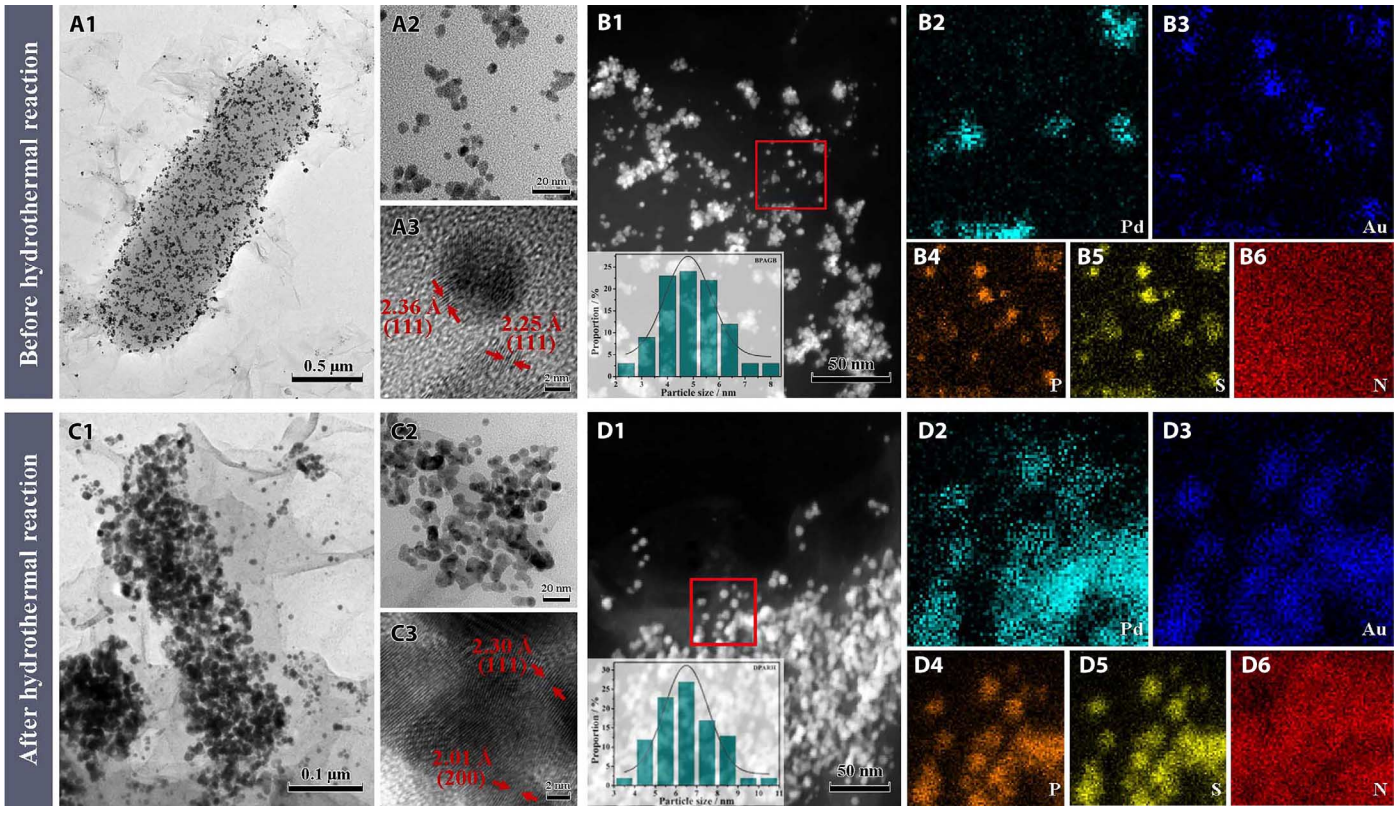

Fig. 3. Morphological features and element distribution of as-prepared materials before and after the hydrothermal reaction. TEM (**A1**) and HRTEM (**A2** and **A3**) imaging and HAADF-STEM elemental mapping (**B1** to **B6**) of BPAGB. TEM (**C1**) and HRTEM (**C2** and **C3**) imaging and HAADF-STEM elemental mapping (**D1** to **D6**) of DPARH after hydrothermal reaction.

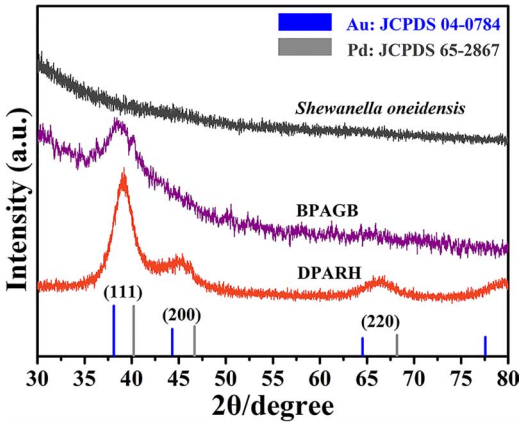

Fig. 4. Structure features. XRD pattern of *S. oneidensis* MR-1, BPAGB, and DPARH. a.u., arbitrary units.

sensitivity factors. The atomic ratio of Pd, Au, P, N, and S elements is 32.28:10.83:4.32:47.09:5.48 (fig. S3 and table S2). On the basis of this result, the mass ratio of Pd and Au is 62:38, which is similar to that tested by inductively coupled plasma atomic emission spectroscopy (67:33).

In previous studies, the rGO was proven to be better than GO in conduction (*49*, *50*), indicating that the reduction of GO can greatly influence the electrocatalytic performance, which was supported by Raman tests. As shown in fig. S4, each of the Raman spectra shows two visible bands. The D band at around 1330 cm^{-1} is related to the partially disordered structures or the structural defects of graphene, whereas the G band at about 1590 cm^{-1} corresponds to the ordered sp2 bonded carbon. The D/G intensity ratio of DPARH, BPAGB, GO, and rGO are 1.27, 1.03, 0.73, and 1.26, respectively, indicating that, in the synthesis process of DPARH, the GO is partly reduced by bacteria and further reduced after the hydrothermal reaction (*51*, *52*).

The electrochemically active surface areas of DPARH and commercial Pd/C catalysts were evaluated by calculating CO stripping experiment results from cyclic voltammograms (CVs) and tested in 0.1 M $HClO_4$ (fig. S5). By assuming that the oxidation of a monolayer of CO on Pd corresponds to a charge of 420 μC cm^{-2} and by normalizing the result by Pd loading amount, the electrochemically active surface areas of DPARH were calculated to be 55.66 m^2 g^{-1}, which is similar to those of commercial Pd/C (52.65 m^2 g^{-1}).

Much higher electrocatalytic activity and durability were achieved by optimizing the synthesis conditions, such as Pd/Au ratio, GO amount, temperature, and time of hydrothermal reaction. The DPARH with Pd/Au ratio of 3:2, coated with GO (10 ng/liter) and synthesized at 200°C for 6 hours, showed the best electrocatalytic performance (figs. S6 and S7 and table S3). The electrocatalytic activity of Pd-based catalyst is affected by its composition because of the changes in the surface

electronic structure of Pd, which has been proven in many previous studies (*12*, *40*). Hydrothermal temperature and treatment time mainly contribute to a different degree of carbonization, resulting in a different electrical conductivity. With increasing hydrothermal temperature and treatment time, the carbonization of bacteria is gradually complete, thus increasing their electrical conductivity and electrocatalytic performance. It should be noted that, with the treatment time increased to 9 hours, the electrocatalytic performance is slightly decreased, which may be attributed to the aggregation of nanoparticles. In addition, the amount of GO also affects the catalytic performance, and it can be mainly attributed to the exposure of surface active sites. When there is little GO in the catalyst, it is hard to build the 3D structure and impossible to avoid the aggregation of nanoparticles, just like the case without GO. However, with an excessive amount of GO, those PdAu nanoparticles would be enclosed by thick GO, preventing the interaction between the small organic molecules and the PdAu active site, which

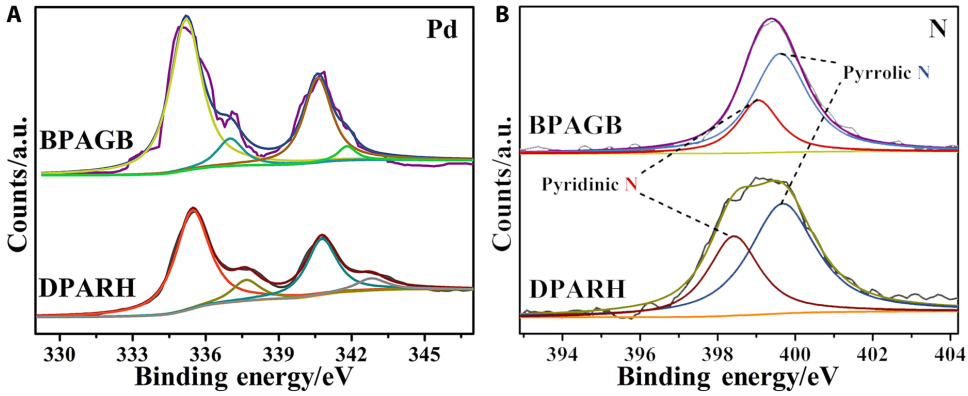

Fig. 5. Surface atom features. XPS of BPAGB and DPARH.

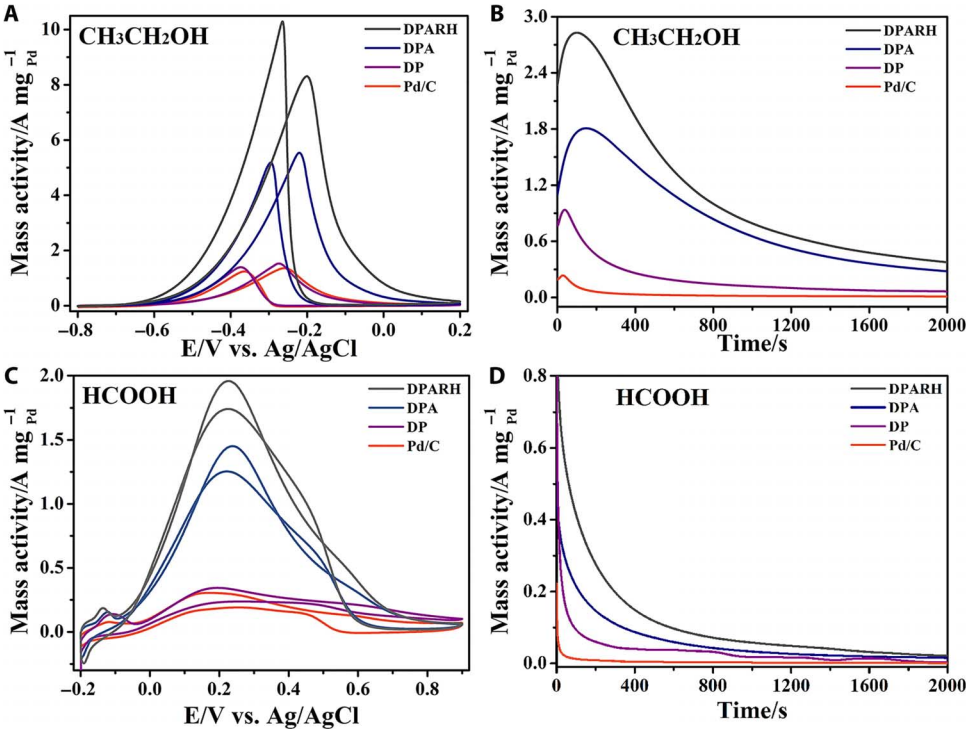

Fig. 6. Detailed electrocatalytic performances of as-prepared catalysts. (**A**) CVs of the DPARH-, DPA-, DP-, and commercial Pd/C catalyst–modified electrodes in 1 M KOH + 1 M ethanol at a scan rate of 50 mV s^{-1} versus Ag/AgCl (saturated KCl). (**B**) Chronoamperometric curves of these catalyst-modified electrodes in 1 M KOH + 1 M ethanol at −0.3 V for 2000 s. (**C**) CVs of these catalyst-modified electrodes in 0.5 M H_2SO_4 + 0.5 M HCOOH at a scan rate of 50 mV s^{-1}. (**D**) Chronoamperometric curves of these catalyst-modified electrodes in 0.5 M H_2SO_4 + 0.5 M HCOOH at 0.1 V for 2000 s. The Pd mass amounts of all the catalysts were about 1 μg in each electrode.

decreases their catalytic activity. To gain a better understanding of the excellent electrocatalytic performance of DPARH, the products, such as DPA and heteroatom-doped bio-Pd (DP), obtained from the process of fabricating DPARH, were also investigated. As illustrated by the CV in Fig. 6 (A and C), the performances of the DP-, DPA-, and DPARH-modified electrodes were gradually improved under both alkaline and acidic conditions. The forward anodic peak current is considered to represent the activity of catalyst. The DP has the lowest activity in our as-prepared catalysts, which is similar to that of commercial Pd/C. With the addition of the Au element, the catalytic activity of DPA showed a 4.1-fold increase (5.54 A mg^{-1}) over that of Pd/C in ethanol oxidation and a 4.7-fold (1.45 A mg^{-1}) increase in formic acid oxidation, indicating that alloying with the Au element tremendously enhances the single Pd catalysts. Moreover, DPARH shows the highest activity in terms of peak current (8.30 A mg^{-1} in ethanol electrooxidation and 2.04 in A mg^{-1} formic aicd electrooxidation). The further enhanced catalytic activity might be mainly attributed to the large surface area of the 3D porous structure with GO coating in DPARH. In addition, the onset potential in the forward scan of ethanol oxidation on DPARH exhibited significantly higher negative shift than that on commercial Pd/C. During the period of ethanol electrooxidation, the dissociative adsorption of ethanol to adsorbed CO_{ads} and CH_x species usually takes place at lower potentials, leading to the complete oxidation of ethanol to CO_2. The negative shift of the onset potential indicates that ethanol is more easily oxidized by DPARH, which is concordant with a previous study reporting that the functionalization of N-doping in carbon support could markedly enhance the kinetics of the ethanol electrooxidation (*53*, *54*).

To further test the stability of the DPARH catalyst, long-term chronoamperometric measurement technique was carried out. From the response curves shown in Fig. 6 (B and D), it can be learned that the Au element can efficiently avoid the current decay and maintain the high electrocatalytic activities of DPARH and DPA for a much longer time than that of DP and commercial Pd/C. This is likely to be attributed to the fact that the gold component can effectively prevent the poisoning of the intermediate species (*40*). Moreover, the PdAu nanoparticles are fixed on the 3D porous skeleton built by GO, which also benefits the durability of DPARH. Both activity and durability experiment results prove that the DPARH is a promising electrocatalyst for the electrooxidation of ethanol and formic acid.

CONCLUSION

Here, an excellent electrocatalyst was fabricated for small organic molecular electrooxidation under both acid and alkaline conditions using the biologically mediated method. The electrochemically active bacterium replaced the toxic surfactant, stabilizer, and chemical reducing agent and in situ–synthesized bio-PdAu nanoparticles on its surface, extending the function of bacteria in three ways: (i) reducing metal ions, (ii) supporting material, and (iii) doping heteroatom. The hydrothermal reaction serves a quadruple purpose in the synthesis process: carbonizing bacterial cells, alloying Pd and Au nanoparticles, functionalizing carbon supports, and reducing GO. Because of its 3D porous structures, alloy nature, carbon support, and heteroatom doping, the DPARH showed an excellent electrocatalytic activity and durability toward ethanol and formic acid oxidation compared with the commercial Pd/C and many other chemically synthesized catalysts. This study offers a new perspective about the utilization of bionanoparticles to markedly accelerate the energy conversion on the anode of fuel cells.

MATERIALS AND METHODS

Chemicals

Tetrachloroauric(III) acid hydrate [$HAuCl_4{\cdot}4H_2O$, analytical grade (AR)], palladium(II) chloride ($PdCl_2$, AR), potassium dihydrogen phosphate (KH_2PO_4, AR), disodium hydrogen phosphate dodecahydrate (Na_2HPO_4, AR), ammonium chloride (NH_4Cl, AR), magnesium sulfate ($MgSO_4$, AR), sodium chloride (NaCl, AR), ammonium sulfate [$(NH_4)_2SO_4$, AR], nitrilotriacetic acid [$N(CH_2CO_2H)_3$, AR], iron(II) sulfate heptahydrate ($FeSO_4{\cdot}7H_2O$, AR), manganese(II) chloride tetrahydrate ($MnCl_2{\cdot}4H_2O$, AR), cobalt(II) chloride hexahydrate ($CoCl_2{\cdot}6H_2O$, AR), copper(II) sulfate pentahydrate ($CuSO_4{\cdot}5H_2O$, AR), zinc chloride ($ZnCl_2$, AR), nickel(II) chloride hexahydrate ($NiCl_2{\cdot}6H_2O$, AR), boric acid (H_3BO_3, AR), aluminum potassium sulfate dodecahydrate [$AlK(SO_4)_2{\cdot}12H_2O$, AR], and sodium molybdate dihydrate ($Na_2MoO_4{\cdot}2H_2O$, AR) were purchased from Sinopharm Chemical Reagent Co. Ltd. Sodium selenite (Na_2SeO_3, 98%) and sodium tungstate dihydrate purum ($NaWO_4{\cdot}2H_2O$, 99%) were supplied by Sigma-Aldrich. In all of the experiments, ultrapure water with a conductivity of 18.2 megohm·cm was used to dissolve and dilute chemical reagents.

Bacterial culture

S. oneidensis MR-1 was obtained from the American Type Culture Collection and was incubated in LB medium (pH 7.0) at 30°C with shaking at 120 rpm for 24 hours. Then, *S. oneidensis* MR-1 cells were concentrated by centrifugation at 6000 rpm for 5 min and washed twice with sterilized buffer [pH 7.0; KH_2PO_4 (3 g/liter), Na_2HPO_4 (6 g/liter), NH_4Cl (1 g/liter), NaCl (0.5 g/liter), $CaCl_2$ (0.011 g/liter), $MgSO_4$ (0.012 g/liter)]. Finally, the washed *S. oneidensis* MR-1 cells were resuspended into 20 ml of buffer and purged with nitrogen gas to remove the dissolved oxygen.

Synthesis of BP and DP

Sodium lactate [2 ml; 60% (w/w)] was added into 1 liter of M9 buffer and purged with nitrogen gas to form the reaction solution. Cell resuspension solution (1 ml) was injected into 24 ml of as-prepared reaction solution, followed by injecting 100 μl of 40 mM H_2PdCl_4. After shaking it for 1.5 hours, the BP was synthesized and washed in 0.5% NaCl solution.

The as-prepared BP was resuspended into a Teflon autoclave with 20 ml of water and treated at 200°C for 6 hours. After cooling down to room temperature, the DP was fabricated and washed in 50% alcohol solution, followed by dispersion into 1 ml of 50% alcohol solution for storage.

Synthesis of BPA and DPA

These BPA and DPA were synthesized as described above for the fabrication of BP and DP. The only difference was that at t = 0.5 hours in the synthesis of BP, 50 μl of 20 mM $HAuCl_4$ was injected into the reaction solution.

Synthesis of BPABG and DPARH

These BPABG and DPARH were synthesized as described above for the preparation of BPA and DPA, except that at t = 1 hour in the synthesis

of BPA, 250 µl of GO (1 mg/ml) was also injected into the reaction solution.

Morphological characterization

Materials for SEM analysis were resuspended in 2.5% (w/v) glutaraldehyde phosphate-buffered solution (100 mM, pH 7.0) for 24 hours. Then, the silicon slice coated with Formvar film was added into dispersed solution [phosphate-buffered solution (100 mM, pH 7.0)] of materials for 2 hours. After washing three times with phosphate-buffered solution (100 mM, pH 7.0), the cells were fixed again in 2.5% (w/v) glutaraldehyde for 1 hour. Next, the cells were dehydrated in a gradient ethanol series (30% twice, and 50, 70, 90, 95, and 100% twice) for 15 min each. After drying at 60°C for 12 hours, the cells were placed onto a carbon substrate for SEM observation (S-4800 FE-SEM, Hitachi).

Samples for TEM analysis were prepared by dripping a single drop of diluted sample dispersion on copper grids. A JEM-2100F HRTEM equipped with an accelerating voltage of 200 kV was used to record the HRTEM images. STEM elemental maps were made on a FEI TECNAI F30 microscope operated at 300 kV under the HAADF mode.

Structure characterization

The XRD analysis of all the samples was accomplished with a Bruker D8 Advance x-ray diffractometer equipped with a Cu Kα radiation source. XPS experiments were measured by a Thermo VG Multilab 2000 spectrometer equipped with a monochromatic Al Kα radiation source at room temperature. Inductively coupled plasma atomic emission spectroscopy (ICP-AES) was tested by Optima-7000DV (PerkinElmer).

Electrochemical measurement

The electrochemical measurements of ethanol and formic acid electrooxidation reaction were performed in a three-electrode cell consisting of a glassy carbon (GC; 5 mm in diameter), an Ag/AgCl (saturated KCl) reference electrode, and a platinum wire counter electrode using CHI 660E electrochemical workstation (CH Instruments Inc.). The GC electrode was successively polished with 1.0-, 0.3-, and 0.05-µm alumina powder and washed with deionized water, followed by sonication in 8 M HNO_3, ethanol, and deionized water, respectively, before the electrochemical experiments. Then, the electrode was dried under nitrogen atmosphere. For all the electrocatalytic tests, 4 µl of as-prepared catalysts and commercial Pd/C catalyst ethanal aqueous solution [1:1 ($v_{ethanal}$:v_{water})] were dropped on the surface of each electrode and dried at room temperature. Then, 5 µl of 0.028% Nafion (diluted from 5% Nafion by ethanol; Sigma-Aldrich) was added and dried before the experiment. The Pd mass amounts of all the tested catalysts on each GC electrode were almost 1 µg, which were measured by ICP-AES.

SUPPLEMENTARY MATERIALS

Supplementary material for this article is available at http://advances.sciencemag.org/cgi/content/full/2/9/e1600858/DC1

fig. S1. The mechanism of biosynthesis.
fig. S2. Morphological feature of different biocatalysts.
fig. S3. Atomic ratio of as-prepared catalyst.
fig. S4. Feature of graphene.
fig. S5. CO stripping for the DPARH and commercial Pd/C.
fig. S6. Ethanol electrooxidation activities of the DPARH synthesized under different conditions.
fig. S7. Formic acid electrooxidation activities of the DPARH synthesized under different conditions.
table S1. Electrocatalytic mass activities of different catalysts in previous studies.
table S2. Atomic ratio of the DPARH from the XPS data.
table S3. Electrocatalytic mass activities of DPARH synthesized under different conditions.
References (*55*–*64*)

REFERENCES AND NOTES

1. M. Winter, R. J. Brodd, What are batteries, fuel cells, and supercapacitors? *Chem. Rev.* **104**, 4245–4269 (2004).
2. B. C. H. Steele, A. Heinzel, Materials for fuel-cell technologies. *Nature* **414**, 345–352 (2001).
3. A. S. Aricò, P. Bruce, B. Scrosati, J.-M. Tarascon, W. van Schalkwijk, Nanostructured materials for advanced energy conversion and storage devices. *Nat. Mater.* **4**, 366–377 (2005).
4. N. Tian, Z.-Y. Zhou, S.-G. Sun, Y. Ding, Z. L. Wang, Synthesis of tetrahexahedral platinum nanocrystals with high-index facets and high electro-oxidation activity. *Science* **316**, 732–735 (2007).
5. X. Huang, S. Tang, X. Mu, Y. Dai, G. Chen, Z. Zhou, F. Ruan, Z. Yang, N. Zheng, Freestanding palladium nanosheets with plasmonic and catalytic properties. *Nat. Nanotechnol.* **6**, 28–32 (2011).
6. C. Bianchini, P. K. Shen, Palladium-based electrocatalysts for alcohol oxidation in half cells and in direct alcohol fuel cells. *Chem. Rev.* **109**, 4183–4206 (2009).
7. H. Lee, S. E. Habas, G. A. Somorjai, P. Yang, Localized Pd overgrowth on cubic Pt nanocrystals for enhanced electrocatalytic oxidation of formic acid. *J. Am. Chem. Soc.* **130**, 5406–5407 (2008).
8. X. Yu, P. Pickup, Recent advances in direct formic acid fuel cells (DFAFC). *J. Power Sources* **182**, 124–132 (2008).
9. Y. Tang, W. Cheng, Nanoparticle-modified electrode with size- and shape-dependent electrocatalytic activities. *Langmuir* **29**, 3125–3132 (2013).
10. Y. Tang, W. Cheng, Key parameters governing metallic nanoparticle electrocatalysis. *Nanoscale* **7**, 16151–16164 (2015).
11. C. Zhu, S. Guo, S. Dong, PdM (M = Pt, Au) bimetallic alloy nanowires with enhanced electrocatalytic activity for electro-oxidation of small molecules. *Adv. Mater.* **24**, 2326–2331 (2012).
12. J. Liu, Z. Huang, K. Cai, H. Zhang, Z. Lu, T. Li, Y. Zuo, H. Han, Clean synthesis of an economical 3d nanochain network of pdcu alloy with enhanced electrocatalytic performance towards ethanol oxidation. *Chemistry* **21**, 17779–17785 (2015).
13. J. Chang, L. Feng, C. Liu, W. Xing, X. Hu, An Effective Pd–Ni_2P/C anode catalyst for direct formic acid fuel cells. *Angew. Chem. Int. Ed. Engl.* **53**, 122–126 (2014).
14. J. W. Hong, Y. Kim, D. H. Wi, S. Lee, S.-U. Lee, Y. W. Lee, S.-I. Choi, S. W. Han, Ultrathin free-standing ternary-alloy nanosheets. *Angew. Chem. Int. Ed. Engl.* **55**, 2753–2758 (2016).
15. Y. Yamauchi, A. Tonegawa, M. Komatsu, H. Wang, L. Wang, Y. Nemoto, N. Suzuki, K. Kuroda, Electrochemical synthesis of Mesoporous Pt–Au binary alloys with tunable compositions for enhancement of electrochemical performance. *J. Am. Chem. Soc.* **134**, 5100–5109 (2012).
16. L. Zhang, Y. Tang, J. Bao, T. Lu, C. Li, A carbon-supported Pd-P catalyst as the anodic catalyst in a direct formic acid fuel cell. *J. Power Sources* **162**, 177–179 (2006).
17. R. Jiang, D. T. Tran, J. P. McClure, D. Chu, A class of (Pd–Ni–P) electrocatalysts for the ethanol oxidation reaction in alkaline media. *ACS Catal.* **4**, 2577–2586 (2014).
18. L.-X. Ding, A.-L. Wang, G.-R. Li, Z.-Q. Liu, W.-X. Zhao, C.-Y. Su, Y.-X. Tong, Porous Pt-Ni-P composite nanotube arrays: Highly electroactive and durable catalysts for methanol electrooxidation. *J. Am. Chem. Soc.* **134**, 5730–5733 (2012).
19. S. Yang, L. Zhi, K. Tang, X. Feng, J. Maier, K. Müllen, Efficient synthesis of heteroatom (N or S)-doped graphene based on ultrathin graphene oxide-porous silica sheets for oxygen reduction reactions. *Adv. Funct. Mater.* **22**, 3634–3640 (2012).
20. D. Wei, Y. Liu, Y. Wang, H. Zhang, L. Huang, G. Yu, Synthesis of N-doped graphene by chemical vapor deposition and its electrical properties. *Nano Lett.* **9**, 1752–1758 (2009).
21. C. Huang, C. Li, G. Shi, Graphene based catalysts. *Energy Environ. Sci.* **5**, 8848–8868 (2012).
22. J. Tang, J. Liu, C. Li, Y. Li, M. O. Tade, S. Dai, Y. Yamauchi, Synthesis of nitrogen-doped mesoporous carbon spheres with extra-large pores through assembly of diblock copolymer micelles. *Angew. Chem. Int. Ed. Engl.* **54**, 588–593 (2015).
23. B. Wu, D. Hu, Y. Kuang, B. Liu, X. Zhang, J. Chen, Functionalization of carbon nanotubes by an ionic-liquid polymer: Dispersion of Pt and PtRu nanoparticles on carbon nanotubes and their electrocatalytic oxidation of methanol. *Angew. Chem. Int. Ed. Engl.* **48**, 4751–4754 (2009).
24. Y. Shao, J. Liu, Y. Wang, Y. Lin, Novel catalyst support materials for PEM fuel cells: Current status and future prospects. *J. Mater. Chem.* **19**, 46–59 (2009).
25. J. Shui, M. Wang, F. Du, L. Dai, N-doped carbon nanomaterials are durable catalysts for oxygen reduction reaction in acidic fuel cells. *Sci. Adv.* **1**, e1400129 (2015).
26. J. Zhang, Z. Xia, L. Dai, Carbon-based electrocatalysts for advanced energy conversion and storage. *Sci. Adv.* **1**, e1500564 (2015).

27. H. B. Yang, J. Miao, S.-F. Hung, J. Chen, H. B. Tao, X. Wang, L. Zhang, R. Chen, J. Gao, H. M. Chen, L. Dai, B. Liu, Identification of catalytic sites for oxygen reduction and oxygen evolution in N-doped graphene materials: Development of highly efficient metal-free bifunctional electrocatalyst. *Sci. Adv.* **2**, e1501122 (2016).
28. X. Chen, G. Wu, J. Chen, X. Chen, Z. Xie, X. Wang, Synthesis of "clean" and well-dispersive Pd nanoparticles with excellent electrocatalytic property on graphene oxide. *J. Am. Chem. Soc.* **133**, 3693–3695 (2011).
29. K. B. Narayanan, N. Sakthivel, Biological synthesis of metal nanoparticles by microbes. *Adv. Colloid Interface Sci.* **156**, 1–13 (2010).
30. S. De Corte, T. Hennebel, J. P. Fitts, T. Sabbe, V. Bliznuk, S. Verschuere, D. van der Lelie, W. Verstraete, N. Boon, Biosupported bimetallic Pd–Au nanocatalysts for dechlorination of environmental contaminants. *Environ. Sci. Technol.* **45**, 8506–8513 (2011).
31. X. Wu, F. Zhao, N. Rahunen, J. R. Varcoe, C. Avignone-Rossa, A. E. Thumser, R. C. T. Slade, A role for microbial palladium nanoparticles in extracellular electron transfer. *Angew. Chem. Int. Ed. Engl.* **50**, 427–430 (2011).
32. V. S. Coker, J. A. Bennett, N. D. Telling, T. Henkel, J. M. Charnock, G. van der Laan, R. A. D. Pattrick, C. I. Pearce, R. S. Cutting, I. J. Shannon, J. Wood, E. Arenholz, I. C. Lyon, J. R. Lloyd, Microbial engineering of nanoheterostructures: Biological synthesis of a magnetically recoverable palladium nanocatalyst. *ACS Nano* **4**, 2577–2584 (2010).
33. L. Xiong, J.-J. Chen, Y.-X. Huang, W.-W. Li, J.-F. Xie, H.-Q. Yu, An oxygen reduction catalyst derived from a robust Pd-reducing bacterium. *Nano Energy* **12**, 33–42 (2015).
34. H. Sun, L. Cao, L. Lu, Bacteria promoted hierarchical carbon materials for high-performance supercapacitor. *Energy Environ. Sci.* **5**, 6206–6213 (2012).
35. Z. Guo, G. Ren, C. Jiang, X. Lu, Y. Zhu, L. Jiang, L. Dai, High performance heteroatoms quaternary-doped carbon catalysts derived from *Shewanella* bacteria for oxygen reduction. *Sci. Rep.* **5**, 17064 (2015).
36. T. J. Park, K. G. Lee, S. Y. Lee, Advances in microbial biosynthesis of metal nanoparticles. *Appl. Microbiol. Biotechnol.* **100**, 521–534 (2016).
37. Y. A. Gorby, S. Yanina, J. S. McLean, K. M. Rosso, D. Moyles, A. Dohnalkova, T. J. Beveridge, I. S. Chang, B. H. Kim, K. S. Kim, D. E. Culley, S. B. Reed, M. F. Romine, D. A. Saffarini, E. A. Hill, L. Shi, D. A. Elias, D. W. Kennedy, G. Pinchuk, K. Watanabe, S. Ishii, B. Logan, K. H. Nealson, J. K. Fredrickson, Electrically conductive bacterial nanowires produced by *Shewanella oneidensis* strain MR-1 and other microorganisms. *Proc. Natl. Acad. Sci. U.S.A.* **103**, 11358–11363 (2009).
38. J. M. Myers, C. R. Myers, Overlapping role of the outer membrane cytochromes of *Shewanella oneidensis* MR-1 in the reduction of manganese(IV) oxide. *Lett. Appl. Microbiol.* **37**, 21–25 (2003).
39. A.-K. Herrmann, P. Formanek, L. Borchardt, M. Klose, L. Giebeler, J. Eckert, S. Kaskel, N. Gaponik, A. Eychmüller, Multimetallic aerogels by template-free self-assembly of Au, Ag, Pt, and Pd nanoparticles. *Chem. Mater.* **26**, 1074–1083 (2014).
40. L. Y. Chen, N. Chen, Y. Hou, Z. C. Wang, S. H. Lv, T. Fujita, J. H. Jiang, A. Hirata, M. W. Chen, Geometrically controlled nanoporous PdAu bimetallic catalysts with tunable Pd/Au ratio for direct ethanol fuel cells. *ACS Catal.* **3**, 1220–1230 (2013).
41. K. Zhang, P. Han, L. Gu, L. Zhang, Z. Liu, Q. Kong, C. Zhang, S. Dong, Z. Zhang, J. Yao, H. Xu, G. Cui, L. Chen, Synthesis of nitrogen-doped MnO/graphene nanosheets hybrid material for lithium ion batteries. *ACS Appl. Mater. Interfaces* **4**, 658–664 (2012).
42. S.-K. Park, A. Jin, S.-H. Yu, J. Ha, B. Jang, S. Bong, S. Woo, Y.-E. Sung, Y. Piao, In situ hydrothermal synthesis of Mn_3O_4 nanoparticles on nitrogen-doped graphene as high-performance anode materials for lithium ion batteries. *Electrochim. Acta* **120**, 452–459 (2014).
43. R. Nie, J. Shi, W. Du, W. Ning, Z. Hou, F.-S. Xiao, A sandwich N-doped graphene/Co_3O_4 hybrid: An efficient catalyst for selective oxidation of olefins and alcohols. *J. Mater. Chem. A* **1**, 9037–9045 (2013).
44. C. Nethravathi, C. R. Rajamathi, M. Rajamathi, U. K. Gautam, X. Wang, D. Golberg, Y. Bando, N-doped graphene–VO_2(B) nanosheet-built 3D flower hybrid for lithium ion battery. *ACS Appl. Mater. Interfaces* **5**, 2708–2714 (2013).
45. L. Sun, L. Wang, C. Tian, T. Tan, Y. Xie, K. Shi, M. Li, H. Fu, Nitrogen-doped graphene with high nitrogen level via a one-step hydrothermal reaction of graphene oxide with urea for superior capacitive energy storage. *RSC Adv.* **2**, 4498–4506 (2012).
46. Y.-H. Lee, K.-H. Chang, C.-C. Hu, Differentiate the pseudocapacitance and double-layer capacitance contributions for nitrogen-doped reduced graphene oxide in acidic and alkaline electrolytes. *J. Power Sources* **227**, 300–308 (2013).
47. J. R. Pels, F. Kapteijn, J. A. Moulijn, Q. Zhu, K. M. Thomas, Evolution of nitrogen functionalities in carbonaceous materials during pyrolysis. *Carbon* **33**, 1641–1653 (1995).
48. D. Guo, R. Shibuya, C. Akiba, S. Saji, T. Kondo, J. Nakamura, Active sites of nitrogen-doped carbon materials for oxygen reduction reaction clarified using model catalysts. *Science* **351**, 361–365 (2016).
49. C. Gómez-Navarro, R. T. Weitz, A. M. Bittner, M. Scolari, A. Mews, M. Burghard, K. Kern, Electronic transport properties of individual chemically reduced graphene oxide sheets. *Nano Lett.* **7**, 3499–3503 (2007).
50. L. Li, M. Chen, G. Huang, N. Yang, L. Zhang, H. Wang, Y. Liu, W. Wang, J. Gao, A green method to prepare Pd–Ag nanoparticles supported on reduced graphene oxide and their electrochemical catalysis of methanol and ethanol oxidation. *J. Power Sources* **263**, 13–21 (2014).
51. T. Li, N. Li, J. Liu, K. Cai, M. F. Foda, X. Lei, H. Han, Synthesis of functionalized 3D porous graphene using both ionic liquid and SiO_2 spheres as "spacers" for high-performance application in supercapacitors. *Nanoscale* **7**, 659–669 (2015).
52. Y.-C. Yong, Y.-Y. Yu, X. Zhang, H. Song, Highly active bidirectional electron transfer by a self-assembled electroactive reduced-graphene-oxide-hybridized biofilm. *Angew. Chem. Int. Ed. Engl.* **53**, 4480–4483 (2014).
53. P. Wu, Y. Huang, L. Kang, M. Wu, Y. Wang, Multisource synergistic electrocatalytic oxidation effect of strongly coupled PdM (M = Sn, Pb)/N-doped graphene nanocomposite on small organic molecules. *Sci. Rep.* **5**, 14173 (2015).
54. H. Jin, T. Xiong, Y. Li, X. Xu, M. Li, Y. Wang, Improved electrocatalytic activity for ethanol oxidation by Pd@N-doped carbon from biomass. *Chem. Commun.* **50**, 12637–12640 (2014).
55. S. Hu, F. Munoz, J. Noborikawa, J. Haan, L. Scudiero, S. Ha, Carbon supported Pd-based bimetallic and trimetallic catalyst for formic acid electrochemical oxidation. *Appl. Catal. B Environ.* **180**, 758–765 (2016).
56. S. Fu, C. Zhu, D. Du, Y. Lin, Facile one-step synthesis of three-dimensional Pd–Ag bimetallic alloy networks and their electrocatalytic activity toward ethanol oxidation. *ACS Appl. Mater. Interfaces* **7**, 13842–13848 (2015).
57. S. Yao, G. Li, C. Liu, W. Xing, Enhanced catalytic performance of carbon supported palladium nanoparticles by in-situ synthesis for formic acid electrooxidation. *J. Power Sources* **284**, 355–360 (2015).
58. Q. Wang, Y. Liao, H. Zhang, J. Li, W. Zhao, S. Chen, One-pot synthesis of carbon-supported monodisperse palladium nanoparticles as excellent electrocatalyst for ethanol and formic acid oxidation. *J. Power Sources* **292**, 72–77 (2015).
59. N. Su, X. Chen, Y. Ren, B. Yue, H. Wang, W. Cai, H. He, The facile synthesis of single crystalline palladium arrow-headed tripods and their application in formic acid electro-oxidation. *Chem. Commun.* **51**, 7195–7198 (2015).
60. B. Cai, D. Wen, W. Liu, A.-K. Herrmann, A. Benad, A. Eychmüller, Function-led design of aerogels: Self-assembly of alloyed PdNi hollow nanospheres for efficient electrocatalysis. *Angew. Chem. Int. Ed. Engl.* **54**, 13101–13105 (2015).
61. G.-T. Fu, B.-Y. Xia, R.-G. Ma, Y. Chen, Y.-W. Tang, J.-M. Lee, Trimetallic PtAgCu@PtCu core@shell concave nanooctahedrons with enhanced activity for formic acid oxidation reaction. *Nano Energy* **12**, 824–832 (2015).
62. C. Bi, C. Feng, T. Miao, Y. Song, D. Wang, H. Xia, Understanding the effect of ultrathin AuPd alloy shells of irregularly shaped Au@AuPd nanoparticles with high-index facets on enhanced performance of ethanol oxidation. *Nanoscale* **7**, 20105–20116 (2015).
63. D. Bin, B. Yang, F. Ren, K. Zhang, P. Yang, Y. Du, Facile synthesis of PdNi nanowire networks supported on reduced graphene oxide with enhanced catalytic performance for formic acid oxidation. *J. Mater. Chem. A* **3**, 14001–14006 (2015).
64. Y. Wang, Q. He, J. Guo, J. Wang, Z. Luo, T. D. Shen, K. Ding, A. Khasanov, S. Wei, Z. Guo, Ultrafine FePd nanoalloys decorated multiwalled carbon nanotubes toward enhanced ethanol oxidation reaction. *ACS Appl. Mater. Interfaces* **7**, 23920–23931 (2015).

Acknowledgments: We thank Y. Jiang (State Key Laboratory of Physical Chemistry of Solid Surfaces, Department of Chemistry, College of Chemistry and Chemical Engineering, Xiamen University, Xiamen 361005, China) for the help in electrochemical measurement. **Funding:** We acknowledge the financial support from the National Natural Science Foundation of China (21375043, 21175051, and 21322703). **Author contributions:** H.H. and F.Z. proposed the concept, designed the experiments, and supervised the project. J.L., Y.Z., Z.H., and K.C. carried out the experiments. **Competing interests:** The authors declare that they have no competing interests. **Data and materials availability:** All data needed to evaluate the conclusions in the paper are present in the paper and/or the Supplementary Materials. Additional data related to this paper may be requested from the authors.

Submitted 22 April 2016
Accepted 18 August 2016
Published 30 September 2016
10.1126/sciadv.1600858

Citation: J. Liu, Y. Zheng, Z. Hong, K. Cai, F. Zhao, H. Han, Microbial synthesis of highly dispersed PdAu alloy for enhanced electrocatalysis. *Sci. Adv.* **2**, e1600858 (2016).

ScienceAdvances
AAAS

Microbial synthesis of highly dispersed PdAu alloy for enhanced electrocatalysis

Jiawei Liu, Yue Zheng, Zilan Hong, Kai Cai, Feng Zhao and Heyou Han (September 30, 2016)

Sci Adv 2016, 2:.
doi: 10.1126/sciadv.1600858